GLOBAL BIOGEOCHEMICAL CYCLES, VOL. 14, NO. 1, PAGES 389-405, MARCH 2000

# Roles of biology and gas exchange in determining the $\delta^{13}C$ distribution in the ocean and the preindustrial gradient in atmospheric $\delta^{13}C$

R. J. Murnane

Risk Prediction Initiative, Bermuda Biological Station for Research, Ferry Reach, St. George's, Bermuda

J. L. Sarmiento

Program in Atmospheric and Oceanic Sciences, Department of Geosciences, Princeton University, Princeton, New Jersey

**Abstract.** We examine the processes responsible for the distribution of $\delta^{13}C$ in a global ocean model. The dominant sources of gradients are biological processes and the temperature effect on isotopic fractionation. However, in a model without biology developed to examine the temperature effect of isotopic fractionation in isolation, we find an almost uniform $\delta^{13}C$ distribution. Extremely slow $\delta^{13}C$ air-sea equilibration does not permit the surface ocean to come into equilibrium with the atmosphere and $\delta^{13}C$ in the ocean thus becomes well mixed. However biological effects, which are interior to the ocean, are strongly expressed and minimally effected by air-sea exchange. Biological fractionation thus dominates the oceanic $\delta^{13}C$ distribution. An important feature of the model is an extremely large northward transport of isotopic anomaly. The transfer from the ocean to the Northern Hemisphere atmosphere of 120 Pg C ‰ is equivalent in magnitude to the signal that would be generated by a net terrestrial biospheric uptake of $\approx$ 5 Pg C $yr^{-1}$ from the Northern Hemisphere atmosphere, or an $\approx$ 1-2‰ disequilibrium between terrestrial respiration and photosynthesis. Improved ocean model simulations and observational analysis are required to test for the possible existence of such a large oceanic transport of isotopic anomaly.

## 1. Introduction

Measurements of carbon isotopic ratios in atmospheric $CO_2$ and in dissolved inorganic carbon in the ocean provide valuable information that can be used to constrain carbon fluxes between the ocean, atmosphere, and terrestrial biosphere. The additional information provided by $\delta^{13}C$ data is a result of the large fractionation of $^{13}C$ from $^{12}C$ during photosynthesis relative to the small fractionation during air-sea gas exchange [*Ciais et al.*, 1995; *Francey et al.*, 1995; *Keeling et al.*, 1995].

Measurements of $\delta^{13}C$ in the ocean and atmosphere have been used to estimate the uptake of anthropogenic carbon by the global ocean [*Quay et al.*, 1992; *Tans et al.*, 1993] and to infer the existence and cause of a north-south gradient in preindustrial atmospheric $pCO_2$ [*Keeling et al.*, 1989b]. *Keeling et al.* [1989b] used model results to infer that 0.9 Pg C $yr^{-1}$ were transported north across the equator by the preindustrial atmosphere. A N-S gradient in preindustrial atmospheric $pCO_2$ would be supported by the interhemispheric transport of carbon by the ocean. *Broecker and Peng* [1992] used oceanic data to estimate that 0.6 Pg C $yr^{-1}$ were carried south in the Atlantic, revised later by *Keeling and Peng* [1995] to 0.4 Pg C $yr^{-1}$.

While our ocean carbon cycle model transports 0.17 Pg $yr^{-1}$ south across the equator in the Atlantic Ocean, on a global scale this model transports only 0.12 Pg C $yr^{-1}$ south across the equator [*Sarmiento et al.*, 1995; *Murnane et al.*, 1999]. The small amount of global southward transport is a feature seen in other ocean general circulation models [*Sarmiento et al.*, 1999]. A correction for transport of carbon delivered to the ocean from rivers [*Aumont*, 1998] increases the global southward transport by 0.35 Pg C $yr^{-1}$ [*Sarmiento et al.*, 1999]. With these changes, the southward transport of carbon across the equator in our ocean general circulation models is 0.47 Pg C $yr^{-1}$.

Here we examine the oceanic $\delta^{13}C$ cycle through a series of model simulations using the Geophysical Fluid Dynamics Laboratory (GFDL) Modular Ocean Model (MOM) code [*Pacanowski et al.*, 1993] with an embedded carbon cycle model. We investigate the dominant processes controlling the surface and deep ocean distributions of $\delta^{13}C$ in the model and estimate the preindustrial interhemispheric gradient in the $\delta^{13}C$ of atmospheric $CO_2$ that is consistent with the ocean model's interhemispheric transport of isotopic anomaly. The natural cycle of isotopic carbon is based on a steady state preindustrial model of the oceanic carbon cycle [*Sarmiento et al.*, 1995; *Murnane et al.*, 1999]. We also compare to data the changes in model ocean $\delta^{13}C$ produced by the anthropogenic transient. The anthropogenic transient is simulated by changing the atmospheric boundary condition of the model in a manner consistent with historical estimates and measurements of atmospheric $CO_2$ and $\delta^{13}C$ composition.

We use the "carbon pump" approach to quantify the effects of chemistry, biology, and gas exchange on oceanic $\delta^{13}C$ distributions. Two different gas transfer velocities are used to investigate the response of $\delta^{13}C$ to changes in gas exchange kinetics. The



Paper number 1998GB001071
0886-6236/00/1998GB901071$12.00

"standard" models use the *Wanninkhof* [1992] wind speed dependent gas transfer velocity. The "potential" models restore surface ocean concentrations to equilibrium with the atmosphere every time step. The gas transfer velocity in the potential models is $\Delta z/\Delta t$ = 42 m $d^{-1}$, where $\Delta z$ is the surface layer thickness (50 m) and $\Delta t$ is the model time step (~1.5 days). For comparison, in the standard models, the wind speed dependent gas transfer velocity [*Wanninkhof*, 1992] and wind speeds [*Esbensen and Kushnir*, 1981] result in an area-weighted, global mean gas transfer velocity of 3.9 m $d^{-1}$.

The response of $\delta^{13}C$ to changes in carbon solubility due to temperature and salinity variations is studied with a potential solubility model. The response of $\delta^{13}C$ to the combined effects of biology and solubility is studied with a potential ocean biogeochemistry model (OBM). Carbon chemistry is not linear with respect to variations in temperature, salinity, carbon, and alkalinity so that separate simulations of biological and solubility effects cannot be linearly combined to determine the combined effects of biology and solubility. We therefore estimate biological effects on $\delta^{13}C$ from the difference between the potential OBM and solubility models.

This is not the first time that the "pump" approach has been used to analyze carbon distributions in the ocean. *Volk and Hoffert* [1985] attributed the distribution of carbon in the ocean to solubility, soft tissue, and carbonate pumps. *Volk and Liu* [1988] and *Sarmiento et al.* [1995] discussed the effects of the soft-tissue and solubility pumps on carbon cycling for selected regions of the ocean. *Murnane et al.* [1999] used a global ocean model to avoid some of the simplifications made by *Volk and Liu* [1988] and extended their analysis of the carbon pumps to consider preindustrial and anthropogenic components of the carbon cycle.

Below (Section 2) we analyze the processes responsible for the distribution of $\delta^{13}C$ in the model ocean using the pump approach and include in the analysis the effects of gas exchange through the standard and potential models. We first give some background on the carbon cycle model (details are given in the appendix) before examining the effects of gas exchange, chemistry, and biology on $\delta^{13}C$ distributions in the steady state preindustrial ocean. We then analyze the response of modeled oceanic $\delta^{13}C$ to the anthropogenic transient. Finally, we estimate the interhemispheric transport of isotopic anomaly (defined below) by the preindustrial global ocean and its implications for the interhemispheric gradient in the $\delta^{13}C$ of atmospheric $CO_2$.

### 1.1. Model description

We use for our ocean model an annual mean 4° version of the GFDL primitive equation MOM code [*Pacanowski et al.*, 1993]. A description of the original model, its ability to reproduce the observed uptake of $^{14}C$, small modifications to the model, and the impact of these changes on tracer transport are given elsewhere [*Toggweiler et al.*, 1989a; *Toggweiler and Samuels*, 1993a, b]. The total model depth of 5000 m is represented by 12 levels of increasing thickness. The thickness of the top, second, and bottom levels is 50.9, 68.4, and 869 m, respectively.

The relevant biologically active tracers carried in the model are phosphate, dissolved inorganic carbon (DIC), DI$^{13}C$, total alkalinity (TA), labile dissolved organic carbon (LDOC), and LDO$^{13}C$. DIC and LDOC are the sum of $^{12}C$ and $^{13}C$ in each phase. The LDOC fraction represents the DOC that causes upper ocean DOC concentrations to be greater than the relatively constant deep water concentrations. Particulate organic carbon (POC) is modeled implicitly. Details of the model treatment of DIC and LDOC are given by *Murnane et al.* [1999] and the appendix.

The model is forced with annual mean wind stresses [*Hellerman and Rosenstein*, 1983] and buoyancy fluxes determined by restoring the surface levels to annual mean temperatures and salinities based on observations [*Levitus*, 1982]. The long timescales for $CO_2$ mass and isotopic equilibration suggest that seasonal effects on DIC and $\delta^{13}C$ due to air-sea gas exchange will be relatively restricted. The consequences of seasonality on biological processes are likely to be more significant. We are currently working toward the inclusion of seasonality in our carbon models to resolve this ambiguity.

We produce an ocean in dynamic equilibrium with the preindustrial atmosphere by fixing atmospheric $pCO_2$ at 278.2 ppmv (dry atmosphere value) with a $\delta^{13}C$ = -6.52‰ and allowing $CO_2$ and $^{13}CO_2$ to invade the ocean until the globally integrated air-sea fluxes of $CO_2$ and isotopic anomaly are negligible. The relatively precise $pCO_2$ and $\delta^{13}C$ boundary conditions are chosen to match the initial point of the spline fits of observations used in the anthropogenic transient simulation (Section 1.2 and 3).

### 1.2. Anthropogenic Transient

Simulations of the oceanic uptake of anthropogenic carbon are performed by setting the atmospheric $CO_2$ content at a concentration determined from a spline fit to data (Figure 1a). As atmospheric $pCO_2$ increases with time there is a net air-sea carbon flux into the ocean. The anthropogenic carbon component in the ocean model is defined as the difference between the flux or concentration at a given time and the steady state preindustrial value. The atmospheric $CO_2$ concentration history (F. Joos, personal communication, 1992) is based on a spline fit to data from measurements of trapped air bubbles in the South Pole and Siple ice cores [*Neftel et al.*, 1985; *Friedli et al.*, 1986] and atmospheric measurements made at Mauna Loa [*Keeling and Whorf*, 1991] [cf. *Sarmiento et al.*, 1992; *Siegenthaler and Joos*, 1992].

The isotopic history of the anthropogenic transient (M. Bruno, personal communication, 1992) is based on a spline fit to $\delta^{13}C$ values from the analysis of ice cores from Antarctica (Siple) and Greenland (Dye-3) [*Friedli et al.*, 1986], from estimated atmospheric values provided by U. Siegenthaler (personal communication, 1992) that were based on measurements [*Keeling et al.*, 1979; 1989a], and from direct atmospheric measurements (Francey, personal communication, 1995). The $\delta^{13}C$ data are sparse (Figure 1b) compared with $CO_2$ measurements, and the $\delta^{13}C$ spline is not intended to represent an optimal estimate of the atmospheric record.

### 1.3. Units

Isotopic data are usually reported as delta values with per mil units. The delta value, $\delta^{13}C$, represents the departure in per mil units of the sample's $^{13}C/^{12}C$ isotopic ratio, r, relative to a reference standard, $r_{std}$,

$$\delta = \left(\frac{r}{r_{std}} - 1\right) 1000 \cdot \qquad (1)$$

However, the delta value is not conserved in addition and subtraction; we therefore use the "isotopic anomaly" to quantify the flux of $^{13}C$. The isotopic anomaly, *I*, is defined as

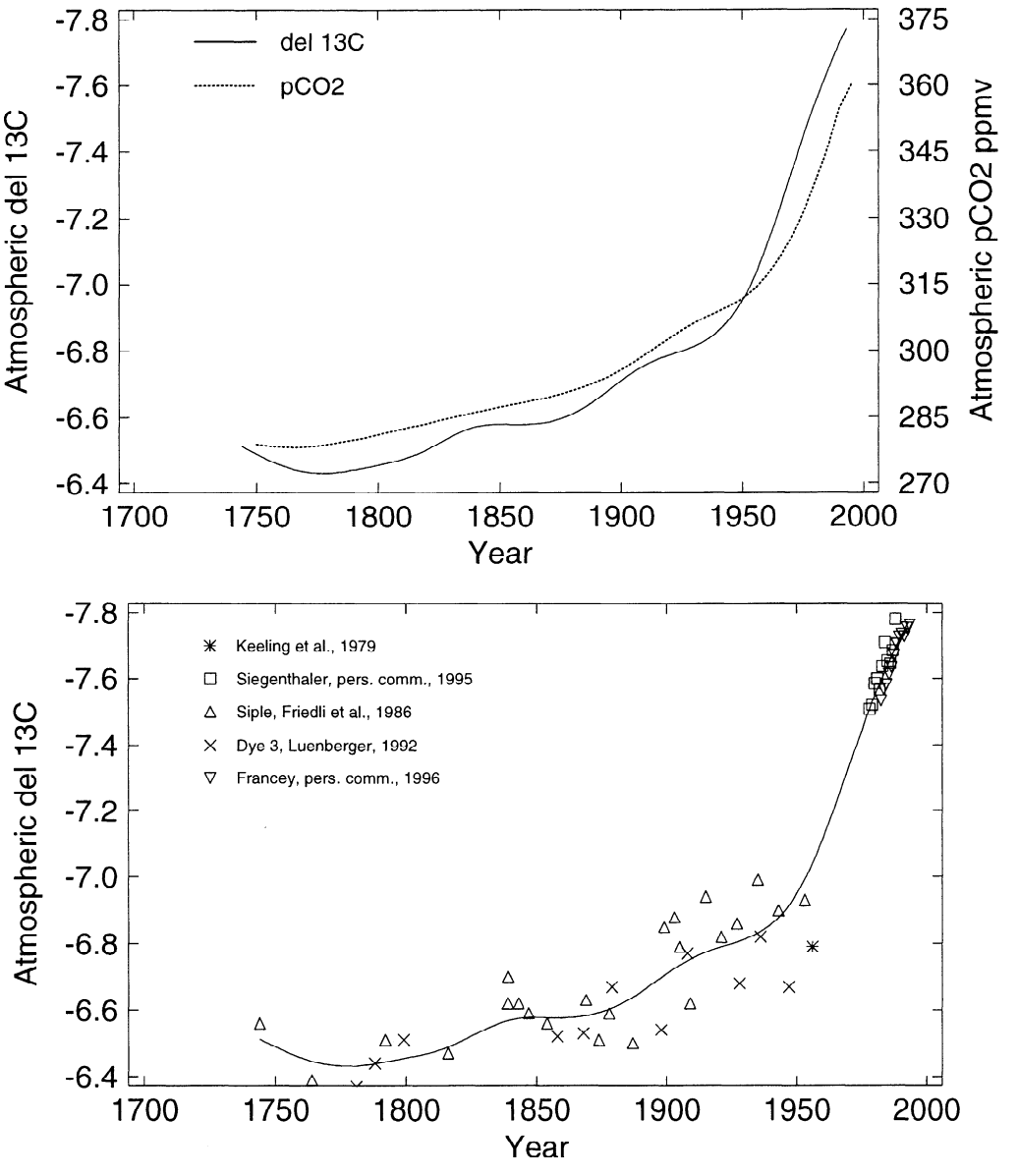


**Figure 1.** (a) Atmospheric history of $pCO_2$ and $\delta^{13}C$ used to force the global ocean carbon cycle model. The scale for $\delta^{13}C$ is reversed to show the correlation between $pCO_2$ and $\delta^{13}C$ changes. (b) Atmospheric [*Keeling et al.*, 1979] and ice core [*Friedli et al.*, 1986; *Leuenberger*, 1992] $\delta^{13}C$ and history (solid line) used to force models. Solid lines in Figures 1a and 1b are identical.

$$I = \left(\frac{R}{R_{std}} - 1\right)1000 = \left(\frac{^{13}C}{R_{std}} - C\right)1000, \quad (2)$$

where $R_{std}$ is the $^{13}C/C$ ratio of $r_{std}$, $R$ is the $^{13}C/C$ ratio of the sample, and $C = {}^{13}C + {}^{12}C$. $I$ is a conservative tracer, as it is a linear combination of C and $^{13}C$, and it has units of Pg C ‰. $I$ is a measure of the departure of $R$ from $R_{std}$ (if $R = R_{std}$, then $I = 0$). A useful approximation is that $I = C\delta^{13}C$ because $^{13}C << {}^{12}C$ and $C \approx {}^{12}C$. The model carries $^{13}C$ and C explicitly so we could present $^{13}C$ and C results directly, but for comparison with data and to exploit the advantages associated with isotopic ratios, we use the approximation $I = C\delta^{13}C$ for the remainder of our discussion. Note that $I$ is a function of $r_{std}$. The usual $r_{std}$ is the Pee Dee Belemnite which has $^{13}C/^{12}C = 0.0112372$.

## 2. Steady State Preindustrial Ocean

Previous studies have proposed that biological processes control deep ocean $\delta^{13}C$ [*Broecker and Maier-Reimer*, 1992; *Lynch-Stieglitz et al.*, 1995] and that "biological effects" cancel "thermodynamic effects" to produce the relatively constant surface ocean $\delta^{13}C$ observed in the modern ocean [*Broecker and Maier-Reimer*, 1992]. In agreement with previous work, we find that biology is the major control on deep ocean $\delta^{13}C$ distributions. However, biology's dominance in the deep ocean of the model is due to the biological signal being overlaid on a relatively uniform background $\delta^{13}C$ distribution produced by the solubility model. The potential effect of the thermodynamic effects, i.e., the potential solubility pump, is quite large, but the signal is

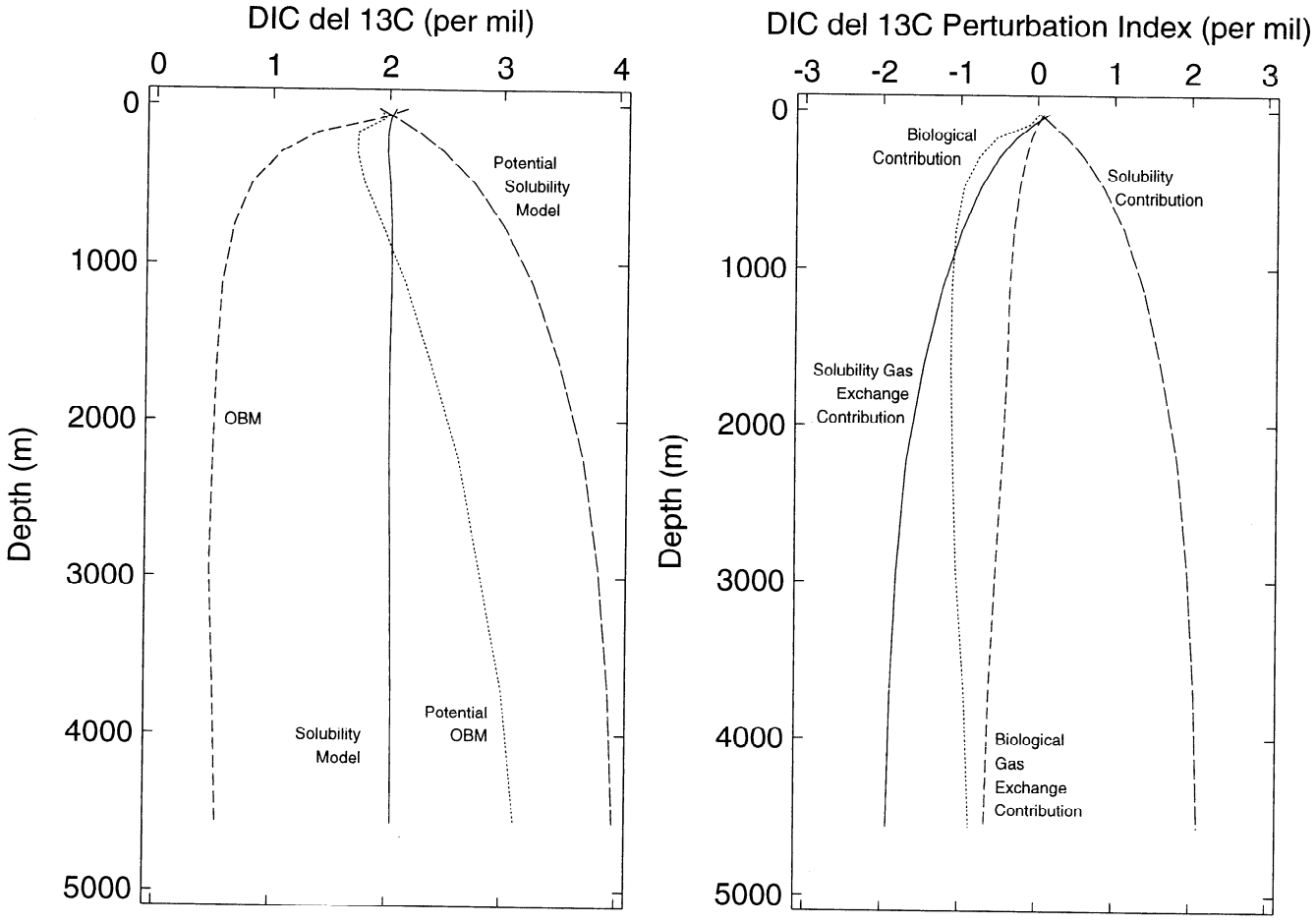


**Figure 2.** (a) DIC $\delta^{13}C$ as a function of depth for the preindustrial: solubility model, potential solubility model, OBM, and potential OBM. (b) The contribution of gas exchange, solubility, or biological processes to the $\delta^{13}C$ versus depth profile for the OBM model (Figure 2a). The sum of all the curves in Figure 2b plus 2.15‰ yields the OBM curve in Figure 2a. The level mean contributions are calculated using equation (3) and the values in Table 1. The 2.15‰ value is the $\delta^{13}C$ for seawater with surface mean $T$ (°C), $S$ (‰), and $TA$ ($\mu$eq kg$^{-1}$) in equilibrium with the preindustrial atmosphere.

smoothed out because of the failure of the surface to equilibrate with the atmosphere. The slow equilibration is a result of the slow gas exchange relative to the rate at which waters in the mixed layer are replaced with waters from below. Furthermore, contrary to the earlier studies, at the surface of the ocean we find that biological effects complement the dominant effects of wind speed dependent gas exchange to drive mean surface ocean $\delta^{13}C$ in the OBM away from thermodynamic equilibrium with the atmosphere.

We proceed by examining the $\delta^{13}C$ distributions produced by solubility, biological, and gas exchange effects. The volume-weighted, level average $\delta^{13}C$ for the potential solubility model increases with depth (Figure 2a) from a value of $\approx$ 2‰ at the surface to $\approx$ 4‰ at depth due to slight differences in the temperature sensitivity of the solubility of the different carbon isotopes. The temperature sensitivity causes DIC in equilibrium with the atmosphere to become isotopically heavier by approximately 1‰ for every 10°C decrease in temperature. The 2‰ increase in $\delta^{13}C$ through the water column is caused by the nearly 20°C range in level mean ocean temperature.

Differences in the temperature dependence of $^{12}C$ and $^{13}C$ solubility controls not only level mean $\delta^{13}C$ but also the spatial distribution of $\delta^{13}C$ in the potential solubility model. The $\delta^{13}C$ contours in zonal mean sections of the potential solubility model (Figure 3) parallel temperature contours. The 30°C range in surface ocean temperatures produces the nearly 3‰ range in surface ocean $\delta^{13}C$ (Figure 4).

The solubility model has a small range in $\delta^{13}C$ values (Figures 2, 3, and 4) relative to the range in the potential solubility model because slow gas exchange essentially caps the ocean and allows it to mix uniformly. The wind speed dependent gas transfer velocity results in a 7 year timescale for $\delta^{13}C$ air-sea equilibration in the topmost 50 m layer. High-latitude surface waters in the solubility model are isotopically lighter than in the potential solubility model because they cool and leave the surface before the wind speed dependent gas transfer velocity allows them to reach isotopic equilibrium with the atmosphere. Low-latitude surface waters in the solubility model are isotopically heavier than in the potential solubility model because they warm and diverge before the wind speed dependent gas transfer velocity allows them to reach isotopic equilibrium with the atmosphere.

Isotopic fractionation of $^{13}C$ from $^{12}C$ during photosynthesis

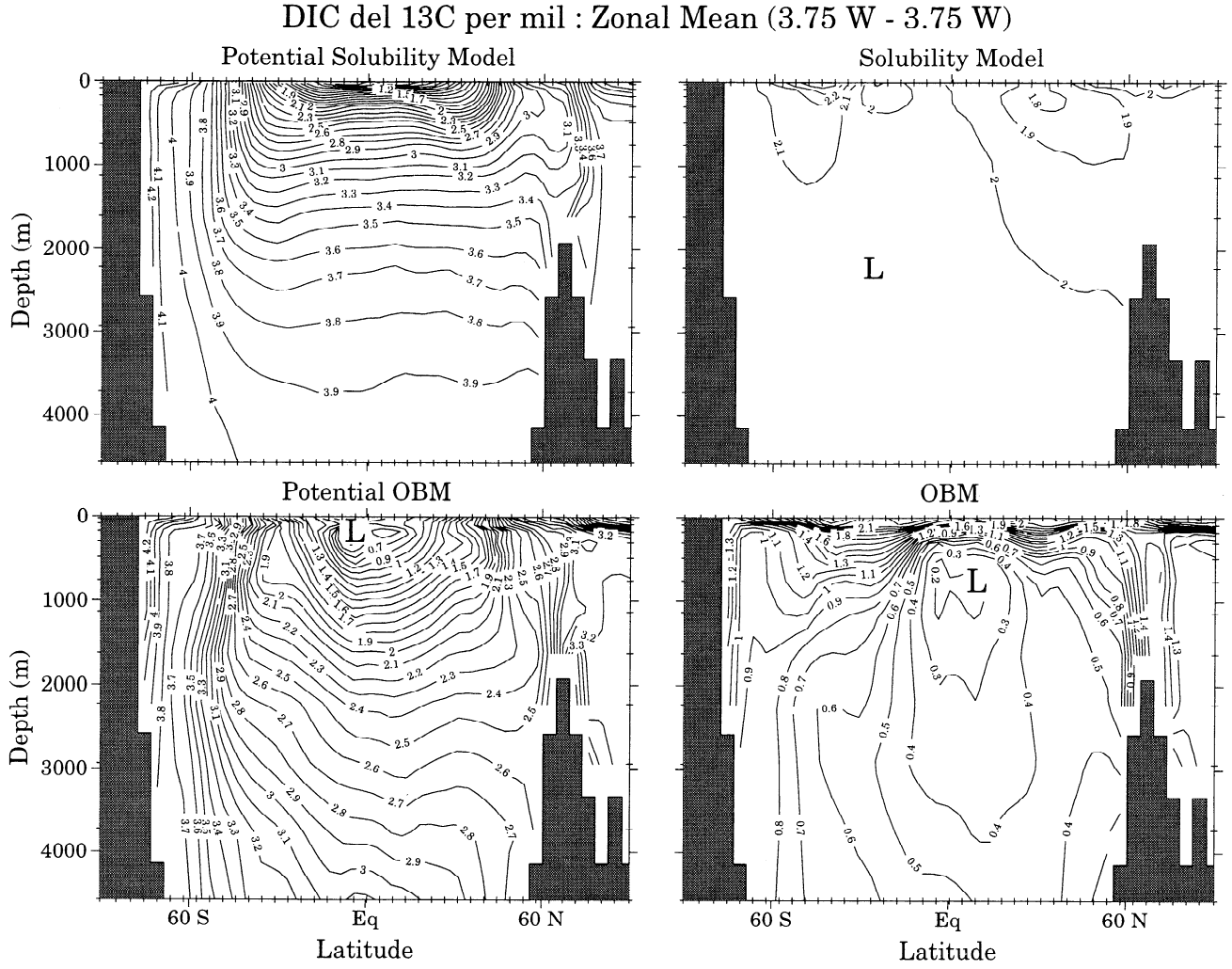


**Figure 3.** Zonal mean $\delta^{13}C$ as a function of depth and latitude. The results are for the preindustrial ocean.

makes POC and LDOC that are –23‰ isotopically lighter than DIC. In the model, isotopic fractionation during carbonate precipitation produces carbonate that is approximately 1‰ heavier than DIC. The net effect of the vertical flux of POC and carbonate from the photic zone and their subsequent remineralization and dissolution is to enrich the deep ocean in isotopically light carbon because 6.3 times more organic carbon than carbonate carbon leaves the model's euphotic [*Murnane et al.*, 1999]. The minimum in potential OBM $\delta^{13}C$ occurs where net remineralization is the highest.

Local and volume-weighted level average surface layer $\delta^{13}C$ in the potential OBM differs little from that in the potential solubility model. Biological production has only a small effect on the surface water parameters that determine the value of $\delta^{13}C$ that is in equilibrium with the atmosphere (Figures 2 and 4). This situation changes dramatically with the OBM. The slow air-sea equilibration time in the OBM prevents the equilibration of surface waters and the atmosphere. In upwelling regions such as the Southern Ocean or eastern equatorial Pacific, surface ocean DIC in the OBM can be more than 0.5‰ lighter than in the solubility model (Figure 4). In regions where export production drives surface nutrients to low concentrations, surface $\delta^{13}C$ in the OBM is more than 0.2‰ heavier than in the solubility model.

The contribution of each effect to the final distribution of $\delta^{13}C$ in the OBM is quantified using an index, $P^{index}(k)$, which gives, in per mil units, the area-weighted horizontal mean difference between a predicted $\delta^{13}C$ and a specified reference value for $\delta^{13}C$:

$$P^{index}(k) = \frac{\int \left(\delta^{13}C_p(i,j,k) - \delta^{13}C_s(i,j,k)\right) dA(i,j)}{\int dA(i,j)}, \qquad (3)$$

where $dA(i,j)$ is the area of grid point $(i,j,k)$, $\delta^{13}C_P(i,j,k)$ is the predicted $\delta^{13}C$ at the grid point $(i,j,k)$, and $\delta^{13}C_S(i,j,k)$ is the specified reference $\delta^{13}C$ value at the grid point (i,j,k). The $\delta^{13}C_S$(i,j,k) are different for each model scenario and chosen so that the value of $P^{index}(k)$ will highlight the contribution of a given process to the overall distribution of $\delta^{13}C$ in the OBM. The $\delta^{13}C_S$ values used to calculate the different indices are listed in Table 1.

The level mean index values calculated with (3) can be used to assess the contribution of specific processes to $\delta^{13}C$ at different

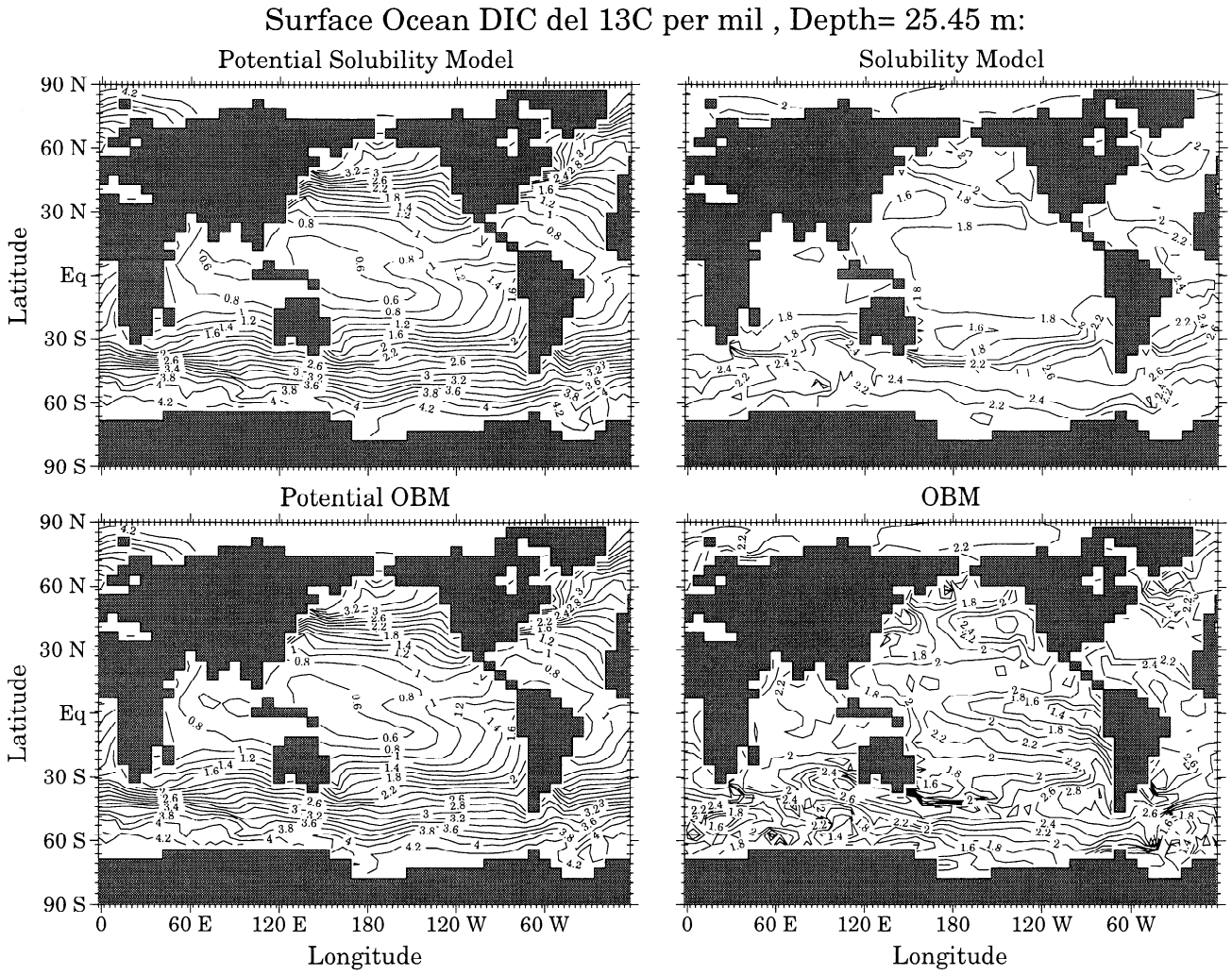


**Figure 4.** Surface ocean DIC $\delta^{13}C$ for the preindustrial ocean predicted with the solubility and OBM potential and standard models.

depths in the OBM (Figure 2b). The solubility contribution increases with depth because water temperatures decrease with increasing depth and the equilibrium $\delta^{13}C$ of DIC becomes heavier with colder temperatures. The negative values for the solubility gas exchange contribution at depth are a result of deep water in the solubility model being produced from high-latitude surface water which is isotopically lighter than potential solubility model surface water (Figure 4). The small positive value for the solubility gas exchange contribution in the surface ocean is due to the large areal extent of low-latitude surface waters with $\delta^{13}C$ values heavier than those in the potential solubility model (Figure 4). The sum of 2.15 plus the solubility contribution plus the solubility gas exchange contribution produces the relatively constant $\delta^{13}C$ profile for the solubility model (Figure 2a).

Below the surface level, the biological contribution to the OBM $\delta^{13}C$ profile (Figure 2b) is negative due to the respiration at depth of isotopically light carbon. At the surface the biological contribution is essentially zero because both the potential OBM and potential solubility model are restored to equilibrium with the atmosphere.

The sum of the biological contribution and biological gas exchange contribution is the primary $\delta^{13}C$ signal seen in the OBM. The primacy of the biological signal is consistent with previous work [*Broecker and Maier-Reimer*, 1992; *Lynch-Stieglitz et al.*, 1995]; however, we find that this primacy occurs because the solubility and solubility gas exchange contributions essentially cancel and tend to produce an ocean with a homogeneous $\delta^{13}C$ distribution. For a fixed amount of biological production, a significant increase in gas transfer velocities will alter the balance between the solubility and the solubility gas exchange contribution and diminish the primacy of the biological signal in the deep ocean.

An examination of the surface ocean distributions of $\delta^{13}C$ predicted with the different model scenarios shows that both wind speed dependent gas transfer velocities and biology drive surface ocean $\delta^{13}C$ away from equilibrium with the atmosphere. The potential solubility model and potential OBM have nearly identical surface ocean $\delta^{13}C$ distributions which vary by more than 3.5‰ (Figure 4 and 5). The wind speed dependent gas transfer velocity in the solubility model produces a relatively

**Table 1.** Specified and Predicted $\delta^{13}C$ Used to Calculate $P^{index}(k)$ and Define the Contribution of a Process to the Distribution of $\delta^{13}C$ in the Model Ocean

| Predicted $\delta^{13}C_P$ | Specified $\delta^{13}C_S$ | Contribution Defined by $P^{index}(k)$ |
|---|---|---|
| Potential solubility model | 2.15 ‰ | solubility contribution |
| Potential OBM | potential solubility model | biological contribution |
| Gas Exchange Analysis | | |
| Solubility model | potential solubility model | solubility gas exchange contribution |
| OBM - potential OBM | solubility model - potential solubility model | biological gas exchange contribution |
| OBM | potential OBM | total gas exchange contribution |

The perturbation index, $P^{index}(k)$, is the area-weighted average of the difference between $\delta^{13}C_P$ and $\delta^{13}C_S$ as defined by equation (3). The first two columns show the specified value and model results used to determine the contribution of solubility effects, biological processes, and gas exchange to the overall distribution of $\delta^{13}C$ in the OBM. The value 2.15‰ equals the $\delta^{13}C$ of seawater in with surface mean T, S, and TA in equilibrium with the preindustrial atmosphere.

constant surface ocean $\delta^{13}C$ which is far from equilibrium with the atmosphere (Figure 5). Biological processes add structure to the relatively constant $\delta^{13}C$ predicted with the solubility model (Figure 4) and drive surface OBM $\delta^{13}C$ even further from equilibrium with the atmosphere (Figure 5).

On the basis of these results, we suggest that the primary factor controlling surface ocean $\delta^{13}C$ distributions is the wind speed dependent gas transfer velocity and that biology is a secondary factor. This is a slightly different interpretation than that given by *Broecker and Maier-Reimer* [1992] who state that biology roughly counters thermodynamic effects. The difference in interpretations can be appreciated by considering two points: (1) Surface ocean $\delta^{13}C$ in the solubility model is far from equilibrium despite the lack of biology to counter thermodynamic (solubility) effects, and (2) the potential solubility model and potential OBM have nearly identical surface ocean $\delta^{13}C$ distributions. The implications of an increase in winds are the same for both interpretations: Air-sea disequilibrium will decrease. Note that the biological gas exchange contribution is much smaller than that of the solubility pump. Thus, for example, the effect of an increased gas exchange rate would be primarily a shift of $\delta^{13}C$ in the same direction as a shift from the solubility model toward the potential solubility model.

## 3. Anthropogenic transient

Two recent papers used oceanic and atmospheric $\delta^{13}C$ data from the 1970 to 1990 period to estimate the oceanic uptake of anthropogenic carbon (Table 2). The first estimated the change in oceanic $\delta^{13}C$ inventory between 1970 and 1989-1991 using oceanic $\delta^{13}C$ measurements from the Pacific and a correlation between $\delta^{13}C$ and $\Delta^{14}C$ to extrapolate results to the global ocean [*Quay et al.*, 1992]. The change in global ocean $\delta^{13}C$ inventory ($\int \delta^{13}C dz$ = -208‰ m), combined with assumptions about the

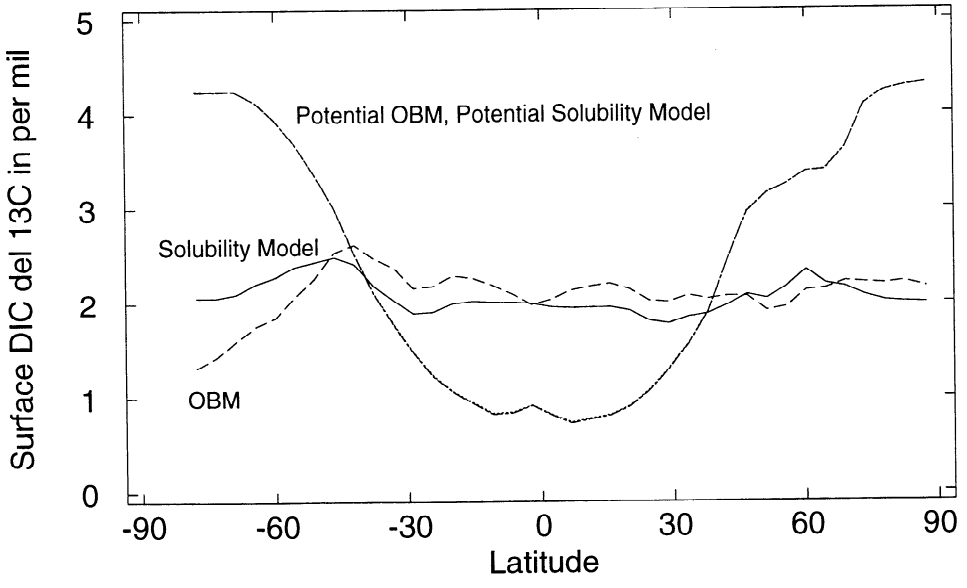


**Figure 5.** Zonal mean $\delta^{13}C$ for the preindustrial surface ocean. The potential solubility model and potential OBM lines appear to be one line because they are nearly identical.

**Table 2.** Summary of Carbon Fluxes and $\delta^{13}C$ Terms in Observations and Models for the 1970-1990 Period

| | $CO_2$ uptake, Pg C $yr^{-1}$ | $^{13}C$ inventory, ‰ m | Air-sea disequilibrium* ‰ | Suess effect ‰ $yr^{-1}$ |
|---|---|---|---|---|
| *Quay et al.* [1992] | 2.1±0.8 | -208±45 | | |
| *Tans et al.* [1993] | 0.2 | | 0.55 | 0.0015+ |
| *Heimann and Maier-Reimer* [1996] | 1.3 | -114 | | |
| *Bacastow et al.* [1996] | 1.4-1.6 | | | -0.0171 |
| This study, OBM | 1.7 | -118 | 0.69, 0.83 | -0.0115 |

* This is for Pacific Ocean only.

\+ These are area weighted values. The two values for the OBM are for 1979 and 1990, respectively.

trend in atmospheric $\delta^{13}C$ and about the terrestrial biosphere, led *Quay et al.* [1992] to suggest that between 1970 and 1990 the ocean absorbed 2.1±0.8 Pg C $yr^{-1}$. The second paper estimated that the ocean absorbed 0.2 Pg C $yr^{-1}$ during the 1970-1990 period using measurements of atmospheric $\delta^{13}C$ and estimates of the global average of air-sea isotopic disequilibrium [*Tans et al.*, 1993]. *Tans et al.* [1993] noted that the 0.2 Pg C $yr^{-1}$ rate of carbon uptake is much smaller than accepted estimates of the order of 2 Pg C $yr^{-1}$ [*Schimel et al.*, 1995].

A third method of estimating anthropogenic carbon uptake from oceanic $\delta^{13}C$ measurements is based on the Suess effect in the surface ocean [*Bacastow et al.*, 1996]. The Suess effect is defined as the rate of change in surface ocean $\delta^{13}C$ through time due to the release of isotopically light anthropogenic carbon to the atmosphere. *Bacastow et al.* [1996] estimate from models and $\delta^{13}C$ observations from the Sargasso Sea that the ocean absorbed 1.4-1.6 Pg C $yr^{-1}$ between 1970 and 1990.

We now compare results from these three papers to model estimates of the change in oceanic $\delta^{13}C$ inventory, air-sea $\delta^{13}C$ disequilibrium, and the $\delta^{13}C$ Suess effect because they are key terms for estimating the oceanic uptake of anthropogenic carbon from $\delta^{13}C$ data. Using the OBM, we predict that between 1970 and 1990 the global ocean absorbed 1.7 Pg C $yr^{-1}$. At the same time the oceanic $\delta^{13}C$ inventory in the OBM changed by -118‰ m (Table 2). The OBM estimate of 1.7 Pg C $yr^{-1}$ uptake between 1970 and 1990 is consistent with the observationally based estimates of *Quay et al.* [1992]; however, the OBM has much smaller changes in $\delta^{13}C$ inventories (Table 2) and surface ocean $\delta^{13}C$ (Figure 6). For comparison, *Heimann and Maier-Reimer* [1996] use the HAMOCC 3 model to predict that between 1970 and 1990 the ocean absorbed 1.3 Pg C $yr^{-1}$ and had a $\delta^{13}C$ inventory change of approximately -114‰ m. Among the probable causes for the different changes in $\delta^{13}C$ inventory estimated with models and observations are poor data quality in the 1970 $\delta^{13}C$ numbers, natural variability in the ocean, ocean model shortcomings, a variable terrestrial biosphere, and an incorrect approximation of the true change in the $\delta^{13}C$ of atmospheric $CO_2$. These are discussed further in what follows.

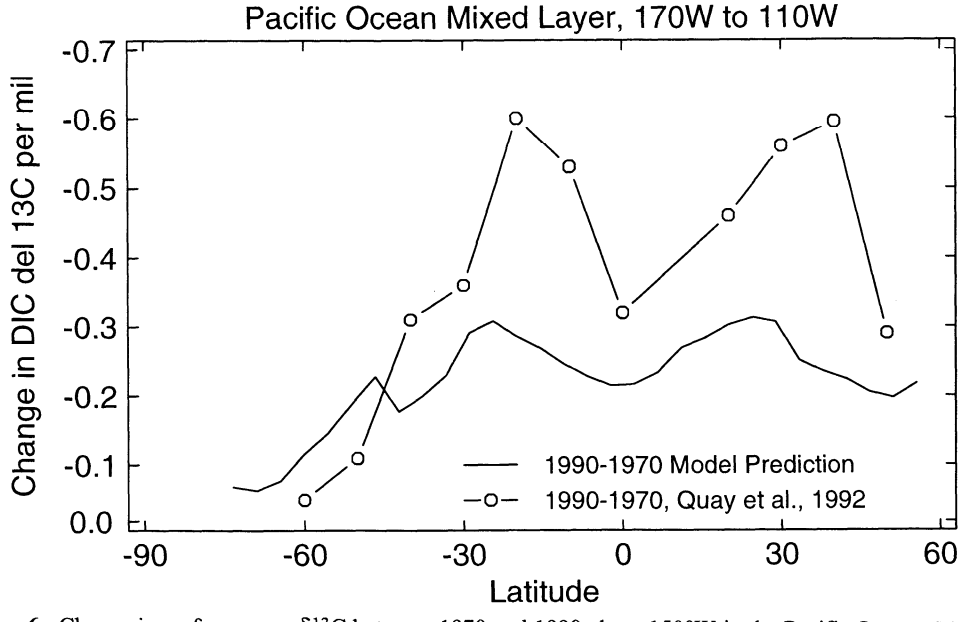


**Figure 6.** Change in surface ocean $\delta^{13}C$ between 1970 and 1990 along 150°W in the Pacific Ocean. Model results are the average of the top two layers. The 1970 model and data values are along 170°W. The 1990 model values 8 south of 6°N are the average of values along 170°W and 150°W, between 8°N and 15°N the values are along 150°W, and north of 15°N the values are along 150°W.

The data shown in Figure 1b are consistent with a relatively wide range of feasible atmospheric $\delta^{13}C$ histories because of the lack of data between the early 1950s and late 1970s and the scatter in the $\delta^{13}C$ data from ice core bubbles. Model studies [*Broecker and Peng*, 1993; *Heimann and Maier-Reimer*, 1996] suggest that the change in surface ocean $\delta^{13}C$ should be of the order of two thirds of the change in atmospheric $\delta^{13}C$. If the -0.4‰ change in surface ocean $\delta^{13}C$ estimated by *Quay et al.* [1992] is correct, then our estimate of the change in the $\delta^{13}C$ of atmospheric $CO_2$ could be too small because the spline fit of Figure 1b gives an atmospheric $\delta^{13}C$ change between 1970 and 1990 of -0.4‰.

Independent evidence for changes in atmospheric $\delta^{13}C$ during the 1970-1990 period comes from studies of air trapped in firn from ice cores in Antarctica which suggest $\delta^{13}C$ decreases by more than 0.4‰ [*Francey et al.*, 1999]. A larger change in the OBM boundary condition for atmospheric $\delta^{13}C$ between 1970 and 1990 would increase the change in the OBM surface ocean $\delta^{13}C$ and be more consistent with the decrease in surface ocean $\delta^{13}C$ estimated by *Quay et al.* [1992] (Figure 6). However, even with a larger decrease in the atmospheric $\delta^{13}C$ boundary condition there will be no difference in anthropogenic carbon uptake by the ocean because carbon uptake in the OBM is independent of the atmospheric $\delta^{13}C$ history.

In the approach developed by *Tans et al.* [1993], the implied oceanic uptake of anthropogenic carbon increases as the air-sea isotopic disequilibrium between the ocean and atmosphere becomes larger. Anthropogenic carbon uptake by the OBM (1.7 Pg C $yr^{-1}$) is greater than that estimated by *Tans et al.* [1993] (0.2 Pg C $yr^{-1}$). Air-sea disequilibrium in the OBM increases through time (from 0.69 to 0.83‰ between 1970 and 1990) and is greater than that estimated by *Tans et al.* [1993] (0.55, Table 2). Air-sea $\delta^{13}C$ disequilibrium is a function of many factors such as air-sea gas exchange rates, surface water residence time, seasonal changes in sea surface temperature, and biology, so the difference in global average air-sea disequilibrium between the OBM and *Tans et al.* estimates cannot be easily analyzed.

*Bacastow et al.* [1996] suggest that the greater the Suess effect the lower the carbon uptake rate. This relationship arises from the fact that if anthropogenic carbon absorbed by the ocean tends to remain close to the surface, then surface ocean $pCO_2$ would be closer to atmospheric values and surface ocean $\delta^{13}C$ lower than if the anthropogenic carbon were mixed to greater depths. Thus trapping anthropogenic carbon near the surface decreases anthropogenic carbon uptake and enhances the Suess effect. *Bacastow et al.* [1996] used data from Bermuda and the Hamburg ocean model to estimate that the global ocean Suess effect is -0.0171‰ $yr^{-1}$ between 1970 and 1990 and that this change in surface ocean $\delta^{13}C$ is associated with the ocean absorbing 1.4-1.6 Pg C $yr^{-1}$ of anthropogenic carbon. The rate of change in the OBM surface ocean $\delta^{13}C$ between 1970 and 1990 is -0.0115‰ $yr^{-1}$. The lower anthropogenic carbon uptake rates of *Bacastow et al.* relative to the OBM are consistent with their more negative Suess effect.

It is difficult to diagnose the cause(s) for the discrepancies between the OBM and other models and observations because the models have different boundary conditions (e.g., surface wind speeds and atmospheric $\delta^{13}C$ history) and numerics (e.g., mixing and advection schemes). The Ocean Carbon Model Intercomparison Project (OCMIP) is one approach that is being used to determine the cause(s) for differences among model predictions [cf. *Sarmiento et al.*, 1999].

A comparison of observations and model results shows that the OBM reproduces many of the general features seen in recently measured $\delta^{13}C$ profiles from a variety of locations (Figure 7). However, more detailed comparisons reveal differences related to shortcomings in the ocean circulation and OBM biology. For example, below 2500 m the North Atlantic Transient Tracers in the Ocean (TTO) $\delta^{13}C$ data tend to be heavier than the model predictions (Figures 7a and 7b) because North Atlantic Deep Water (NADW) in the model is too shallow and there is too much Antarctic Bottom Water (AABW) in the North Atlantic. The large volume and shallow depth of AABW in the North Atlantic causes organic carbon remineralization that normally occurs in NADW to occur in AABW and incorrectly shifts AABW $\delta^{13}C$ to lower than observed values.

In the South Atlantic the model $\delta^{13}C$ differs from observations in the upper kilometer (Figures 7c and 7d). This is due to the combined effects in the model of unrealistic circulation, particularly with respect to convection and intermediate water formation and annual mean biological processes.

In the north Pacific, OBM $\delta^{13}C$ becomes significantly heavier than observed $\delta^{13}C$ (Figures 7e and 7f). Radiocarbon modeling [*Toggweiler et al.*, 1989a, b] suggests that model circulation in the Pacific is fairly realistic. The relatively heavy $\delta^{13}C$ below 1 km of the North Pacific is most likely due to shortcomings in the parameterization of biological processes in the model. Evidence for this is the fact that model phosphate concentrations in the far North Pacific at 1 km depth are almost 0.5 μM below Geochemical Ocean Sections Study (GEOSECS) observations. An increase in deep water phosphate would lower $\delta^{13}C$ by almost 0.5‰ and remedy much of the discrepancy between model predictions and observations.

Phosphate concentrations and $\delta^{13}C$ in the deep ocean of the OBM are linearly related because of the fixed Redfield C:P in organic matter. The slope (-0.86) of the $\delta^{13}C$:phosphate relationship (Figure 8a) for the OBM is less than the observed slope (-1.1) [*Broecker and Maier-Reimer*, 1992]. The cause of the discrepancy probably originates in the function the model uses to predict the $^{13}C$ fractionation factor for the formation of organic matter [*Freeman and Hayes*, 1992]. This fractionation factor is solely a function of $CO_2$ concentrations and OBM $CO_2$ concentrations are always ≤ 20 μM in surface waters. In regions with low-$CO_2$ concentrations, the *Freeman and Hayes* [1992] formulation tends to estimate fractionation factors that are larger than those consistent with observations [*Rau et al.*, 1997]. As a result, the OBM fails to produce POC with $\delta^{13}C$ that spans the observed range of values. For example, in the Southern Ocean the $\delta^{13}C$ of POC does not go below ≈ –27‰ (Figure 8b), whereas observed values range as low as –35‰ [*Goericke and Fry*, 1994]. A more sophisticated model of carbon uptake and fractionation that accounts for intracellular pools [e.g., *Rau et al.*, 1997] could expand the range of modeled $\delta^{13}C$ in POC.

## 4. Preindustrial N-S Gradient in Atmospheric $\delta^{13}C$

The OBM predicts that (1) 0.17 Pg $yr^{-1}$ of DIC are carried southward across the equator in the Atlantic [*Sarmiento et al.*, 1999] and (2) 0.12 Pg $yr^{-1}$ of carbon (DIC and DOC) are trans-

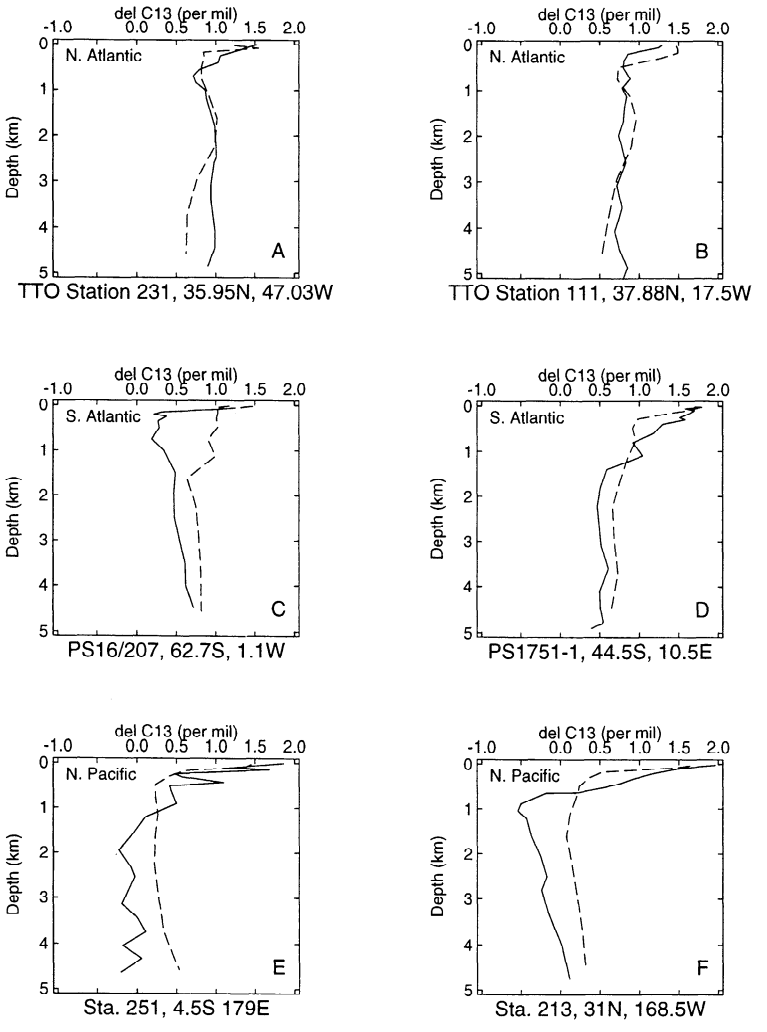


**Figure 7.** Observations versus model results from the Atlantic, Southern Ocean, and Pacific. Observations are solid lines; model results are dashed lines. (a) and (b) Transient Tracers in the Ocean data are from *Lynch-Stieglitz et al.* [1995]; (c) and (d) Polar Stern data are from *Mackensen et al.* [1993], (e) and (f) GEOSECS data are from *Ostlund et al.* [1987].

ported north across the equator on a global scale. Global interhemispheric carbon transport could be enhanced by 0.27-0.43 Pg C $yr^{-1}$ owing to the input of riverine carbon in the Northern Hemisphere that is lost to the atmosphere in the Southern Hemisphere [*Aumont*, 1998]. Despite the small amount of modeled cross-equatorial carbon transport, the OBM predicts that there is a large amount of cross-equatorial transport of isotopic anomaly on a global scale (120 Pg C ‰ $yr^{-1}$). We now examine the implications of this cross-equatorial transport of isotopic anomaly for atmospheric $\delta^{13}C$.

The potential solubility and potential OBM models have essentially no interhemispheric transport of isotopic anomaly because there is no net interhemispheric transfer of heat or nutrients by the ocean model and because $\delta^{13}C$ in the surface ocean and atmosphere are nearly in equilibrium. However, the models with realistic gas transfer velocities transport a significant amount of isotopic anomaly northward across the equator: The solubility model transports 70 Pg C ‰ $yr^{-1}$, and the OBM transports 120 Pg C ‰ $yr^{-1}$. In both models the isotopic anomaly is released to the atmosphere by 30°N (Figure 9). The cross-equatorial transport of isotopic anomaly in the solubility model is a result of a correlation between ocean cooling and strong winds that enhances the net uptake of isotopic anomaly in the Southern Ocean. In the OBM the ventilation of nutrient-rich, isotopically light deep water in the Southern Ocean allows the release of isotopically light $CO_2$ to the atmosphere. This increases the net uptake of isotopic anomaly in the Southern Ocean so that the cross-equatorial transport of isotopic anomaly in the OBM is greater than in the solubility model.

The 120 Pg C ‰ $yr^{-1}$ of isotopic anomaly transported north across the equator in the OBM is released to the atmosphere between 0° and 30°N. The magnitude of this isotopic anomaly flux is equivalent to a terrestrial carbon sink of ≈ 5 Pg C $yr^{-1}$ in the tropical Northern Hemisphere and a terrestrial source of 5 Pg C $yr^{-1}$ in the Southern Hemisphere. The isotopic signal could also be produced by an ≈ 1-2‰ disequilibrium between terrestrial respiration and photosynthetic fluxes. However, it is unlikely that such a large disequilibrium between respiration and photosynthetic fluxes could be produced and maintained.

We estimate how the interhemispheric transport of isotopic

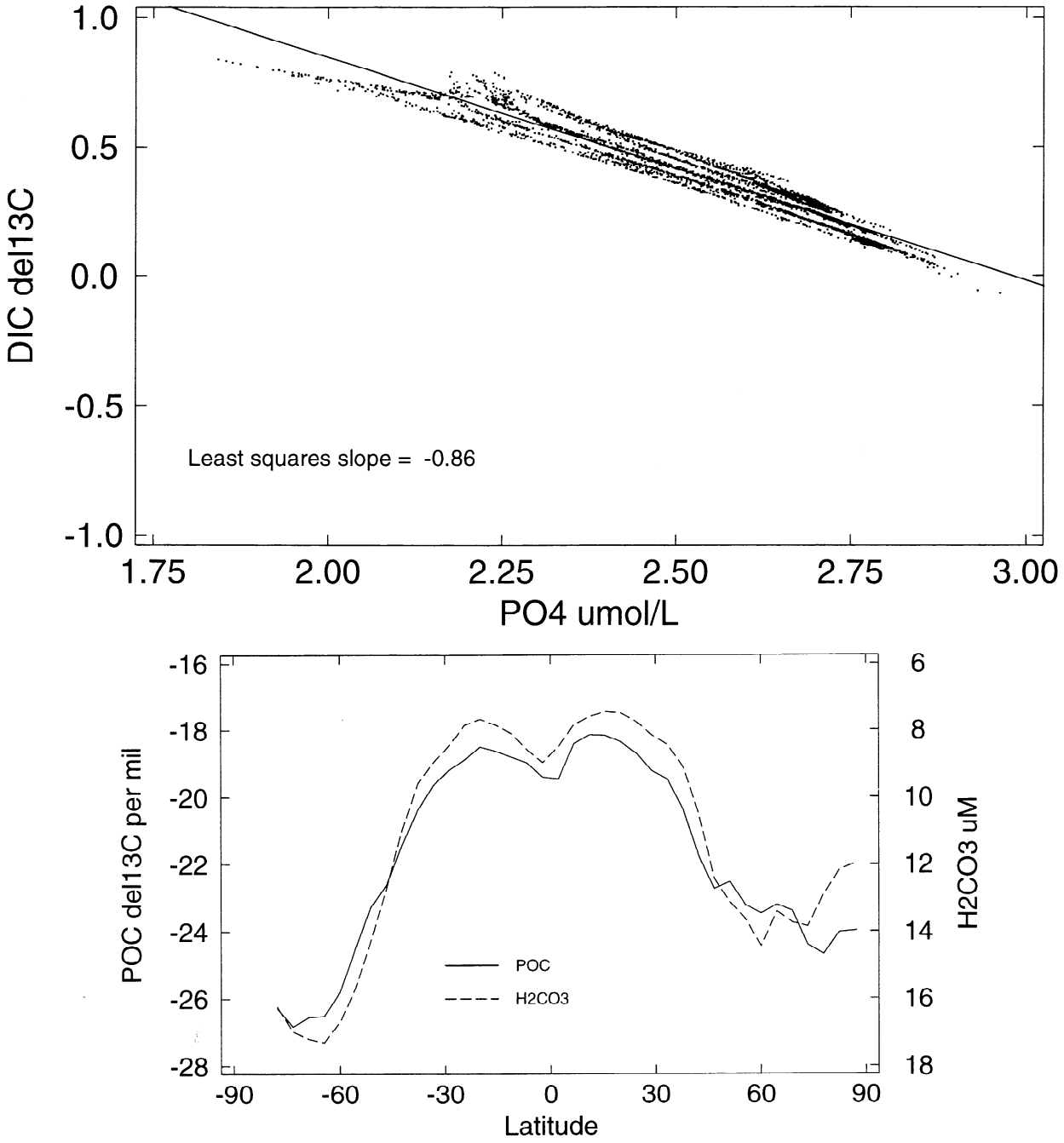


**Figure 8.** (a) Scatter plot showing the relationship between dissolved phosphate and $\delta^{13}C$ in the Indian and Pacific Oceans below 2 km. The slope of -0.86 is significantly less than the observed value of (-1.1) [*Broecker and Maier-Reimer*, 1992]. (b) Zonally averaged values of the $\delta^{13}C$ of POC and of carbonic acid concentrations. The $\delta^{13}C$ of POC in the OBM is directly determined by carbonic acid concentrations. The predicted values in the Southern Ocean do not approach the light values (up to –35‰) seen in observations [*Goericke and Fry*, 1994].

anomaly by the ocean would affect atmospheric $\delta^{13}C$ by using the OBM air-sea fluxes as a boundary condition in a perturbation experiment with the atmospheric general circulation model of *Mahlman and Moxim* [1978]. The interhemispheric transport in the OBM supports an average perturbation to the S-N $\delta^{13}C$ gradient in the atmosphere of approximately -0.07‰ (Figure 10). The zonal mean profile shown in Figure 10 clearly shows the large sink of isotopic anomaly in the Southern Ocean and the source of isotopic anomaly to the atmosphere in the 0°-30°N region. For comparison, the current atmosphere has a S-N $\delta^{13}C$ gradient of ≈ 0.2‰ [*Trolier et al.*, 1996].

*Stephens et al.* [1998] assessed the interhemispheric transport of oxygen and $CO_2$ by the OBM and two additional ocean general circulation models. They used $O_2$ and $CO_2$ air-sea fluxes from each ocean model as boundary conditions for an atmospheric transport model and compared model estimates of atmos-

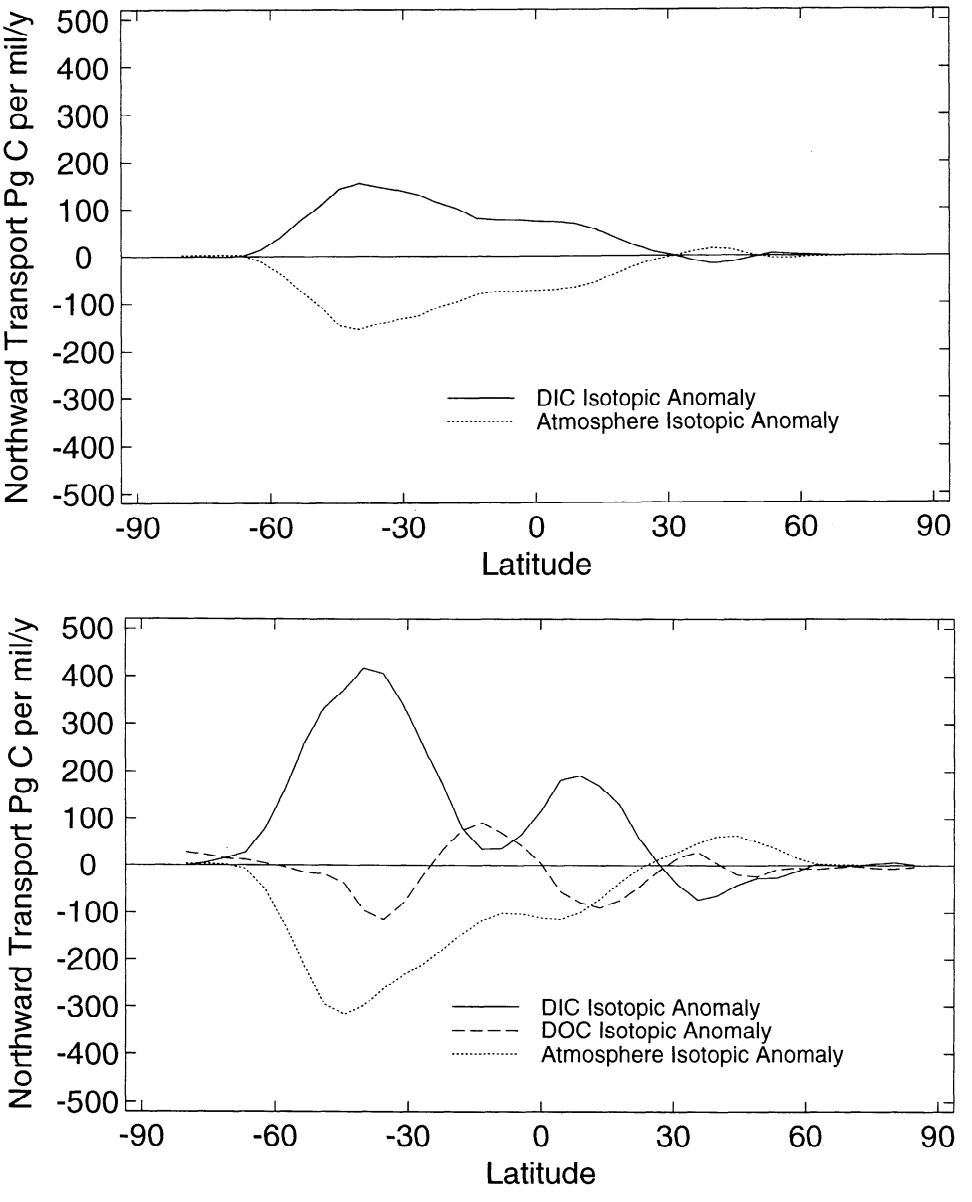


**Figure 9.** Northward transport of isotopic anomaly in the preindustrial ocean by DIC, LDOC, and inferred transport via the atmosphere as derived from air-sea isotopic anomaly fluxes. (a) Solubility model. (b) OBM.

pheric potential oxygen (APO $\approx O_2 + CO_2$) to observations. Their results suggest that all three ocean GCMs underestimate the net southward transport of the sum of $O_2$ and $CO_2$. We cannot determine what effect model shortcoming in interhemispheric transport of $O_2$ and $CO_2$ would have on the interhemispheric transport of isotopic anomaly, but our results on interhemispheric transport of isotopic anomaly and the *Stephens et al.* [1998] study highlights the need for improved simulations of the ocean's interhemispheric transport of oxygen, carbon, and carbon isotopes. To more accurately predict the oceanic transport of isotopic anomaly, the ocean models should have an "interactive" atmosphere with at least three boxes that represent the tropical region, the extratropical Northern Hemisphere, and the extratropical Southern Hemisphere.

## 5. Conclusions

In agreement with earlier work [*Broecker and Maier-Reimer*, 1992; *Lynch-Stieglitz et al.*, 1995], we find that biological effects are the most important factor controlling $\delta^{13}C$ distributions in the deep ocean. However, we find that this dominance is due to the fact that solubility and solubility gas exchange effects essentially cancel in our model (Figure 2b). Biological effects on $\delta^{13}C$ are then overlain on this relatively constant background. In the surface ocean we find that biological effects combine with the effects of the long air-sea equilibration time to drive the surface ocean further from equilibrium with the atmosphere (Figure 5).

The modeled rate of change in surface ocean $\delta^{13}C$ between 1970 and 1990 is -0.0115‰ $yr^{-1}$, nearly half the value (0.02‰)

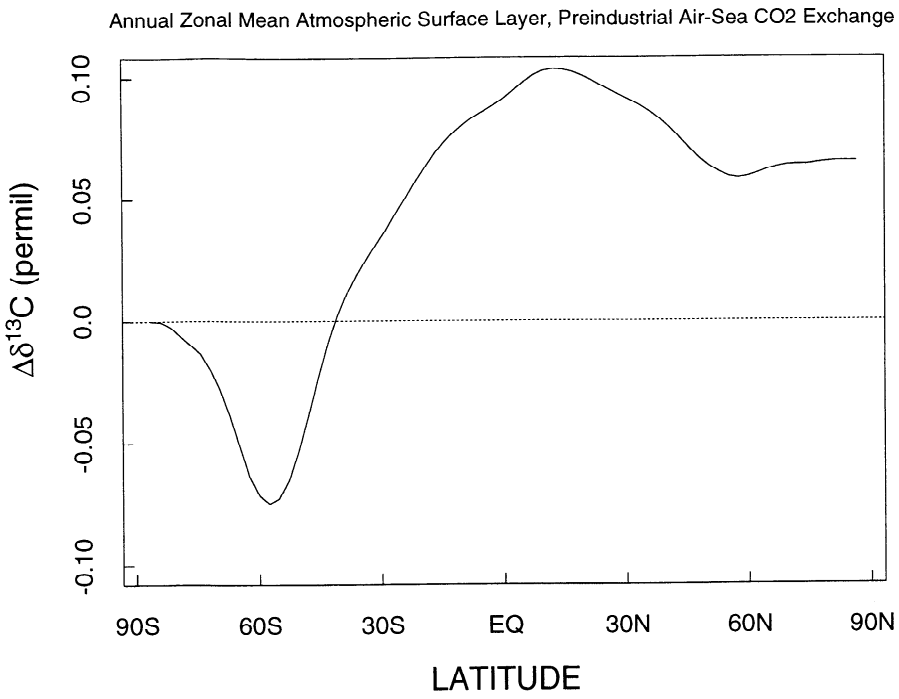


**Figure 10.** The annual zonal mean perturbation to atmospheric $\delta^{13}C$ predicted with an atmospheric general circulation model [*Mahlman and Moxim*, 1978] with boundary conditions set by air-sea fluxes of isotopic anomaly predicted with the OBM. The average S-N interhemispheric gradient is of the order of -0.07‰.

implied by the data by *Quay et al.* [1992] and two-thirds the value predicted by *Bacastow et al.* [1996]. We speculate that the discrepancies between the OBM and Quay et al. results are due to problems with the atmospheric $\delta^{13}C$ boundary condition in the model. We determine the change in the $\delta^{13}C$ of atmospheric $CO_2$ from a spline fit to data from ice core records and atmospheric observations (Figure 1b). A spline fit with different parameters would produce a larger change in atmospheric $\delta^{13}C$ over the 1970-1990 period and increase the change in surface ocean $\delta^{13}C$.

The OBM transports 120 Pg C ‰ of isotopic anomaly northward across the equator. The anomaly is released to the atmosphere by 30°N. The interhemispheric transport of isotopic anomaly is associated with the long air-sea equilibration time for $\delta^{13}C$. There is no interhemispheric transport of isotopic anomaly in the potential models because there is no interhemispheric transport of heat or nutrients, and the ocean and atmosphere are restored to equilibrium at each time step. An atmospheric general circulation model [*Mahlman and Moxim*, 1978] forced by boundary conditions based on air-sea fluxes from the OBM predicts that the ocean fluxes would induce a perturbation in the S-N interhemispheric gradient of atmospheric $\delta^{13}C$ of approximately -0.07‰. If the OBM estimates of isotopic anomaly release to the Northern Hemisphere atmosphere are correct, then neglect of this source of isotopic anomaly in modern carbon budgets would require in the Northern Hemisphere a spurious isotopic disequilibrium between terrestrial respiration and photosynthetic carbon fluxes, an overestimate of terrestrial biosphere carbon sinks in the Northern Hemisphere and sources in the Southern Hemisphere, and/or some mix of these possibilities.

## Appendix

The overall structure of the OBM model equations are described by *Murnane et al.* [1999]. Here we present the modifications that allow the inclusion of $^{13}C$ in the model. We model $^{13}C$ directly rather than the delta values.

The connection between the atmosphere and ocean is established via gas exchange. We model this in the usual way as the product of a gas transfer velocity $k_w$ times the atmosphere-ocean difference in concentrations. The gas transfer velocity for $^{13}C$, $^{13}k_w$, is corrected for kinetic fractionation effects (Table A1) and a -0.2‰ $OH^-$ correction such that

$$\frac{^{13}k_w}{k_w} = 0.9993 \cdot \qquad \text{(A1)}$$

Equilibrium fractionation factors (Table A1) for carbon isotopes in the different DIC species were used to calculate $^{13}CO_2$ in the ocean from the model values of DIC and $DI^{13}C$. The set of chemical reactions that play a role in determining the concentration of $CO_2$ are solved using a procedure analogous to *Peng et al.* [1987] with equilibrium constants summarized in Table A1. The preindustrial atmospheric $^{13}CO_2$ is based on a $\delta^{13}C$ of $CO_2$ set at -6.52‰ and the preindustrial $pCO_2$ = 278.2 ppmv. The fractional ice coverage is the same for $CO_2$ and $^{13}CO_2$.

Simulation of the atmosphere-ocean carbon distribution requires a set of initial conditions. Previous studies have specified the initial total carbon content and maintained it at a constant value throughout the simulation [e.g. *Maier-Reimer and Hasselmann*, 1987; *Bacastow and Maier-Reimer*, 1990, 1991]. Because

**Table A1.** Fractionation Factors and Equilibrium Constants Used for Carbon Chemistry Calculations

| Term | Source or Reference |
|---|---|
| Carbon $K_1$, $K_2$ | *Goyet and Poisson* [1989] |
| Borate K | *Dickson* [1990] |
| Silicate K | *Sjoberg et al.* [1981] |
| Phosphoric Acid $K_1$, $K_2$, $K_3$ | *Dickson and Riley* [1979b] |
| Water K | *Dickson and Riley* [1979a] |
| Ionic strength/salinity relation for seawater | 50.378I = 1.00311S |
| Carbon $\alpha_{g:a}$, $\alpha_{a:b}$, $\alpha_{a:c}$ | *Mook* [1986] |
| Carbon $\alpha_{CaCO3:b}$ | *Rubinson and Clayton* [1969] |
| Carbon $\alpha_{Corg:a}$ | *Freeman and Hayes* [1992] |
| Total Borate+ | S‰11.88 μmol kg$^{-1}$ ‰$^{-1}$ |
| Total Phosphate | 2.15 μmol/kg |
| Total Silica‡ | S‰3.143 μmol kg$^{-1}$ ‰$^{-1}$ |
| Total Sulfate‡ | S‰0.8067 mmol kg$^{-1}$ ‰$^{-1}$ |
| Total Fluorine‡ | S‰1.981 μmol kg$^{-1}$ ‰$^{-1}$ |
| $\beta_{SO4}$ | *Khoo et al.* [1977] |
| $\beta_{HF}$ | *Dickson and Riley* [1979b] |
| Carbon kinetic gas fractionation | *Siegenthaler and Münnich* [1981] |

Fractionation factors for $^{13}C/(^{12}C+^{13}C)$, $^{13}\alpha^*$, are calculated from cited fractionation factors using the relationship $^{13}\alpha^* \approx (^{13}\alpha+0.0112372)/(1+0.0112372)$. The different species for carbon are specified as *g*, *a*, *b*, and *c* and represent gaseous $CO_2$, $CO_2$, $HCO_3^-$, and $CO_3^{2-}$, respectively.

\+ Based on boron/chlorinity relationship of *Uppström* [1974].

‡ Based on mean water concentrations given by *Quinby-Hunt and Turekian* [1983].

of errors in observations and the models, this approach generally leads to a different value of atmospheric and oceanic $pCO_2$ and $\delta^{13}C$ than desired. An important constraint on the model simulations is that we would like to reproduce the preindustrial atmospheric $pCO_2$ and $\delta^{13}C$ so that we can use the models as an initial condition for simulations of the time history of the anthropogenic transient. One way to do this is to run several simulations with different initial carbon inventories until one is found that gives the desired result. A more simple approach, which we adopt, is to fix atmospheric $pCO_2$ and $\delta^{13}C$ at a specified value and allow it to invade the ocean. Equilibrium is achieved when the globally integrated net $CO_2$ and $^{13}CO_2$ sea-air fluxes are negligible. Our approach guarantees that the final total carbon distributions obtained at equilibrium will be consistent with the specified preindustrial atmosphere.

The biogeochemical $^{13}C$ tracer equation solved by the ocean circulation model is

$$\Gamma(C) = J(C)\,; \qquad \text{(A2)}$$

where the time rate of change and transport operator $\Gamma(C)$ is

$$\Gamma(C) = \frac{\partial C}{\partial t} + \mathbf{V}\bullet\nabla C - \nabla_h\bullet(\mathbf{K}_h\nabla_h C) - \frac{\partial}{dz}\left(\frac{K_v}{\delta}\frac{\partial C}{\partial z}\right) \qquad \text{(A3)}$$

and $J$ represents the combination of all in situ sources minus sinks. The tracer concentration is represented by C, **V** is velocity, $\nabla$ is the divergence operator, and **K** is the diffusion tensor. The diffusion term is separated into a horizontal (subscript $h$) and vertical (subscript $v$) component. The parameter $\delta$ is 1, except when two adjacent layers are gravitationally unstable with respect to each other, in which case the two layers are homogenized (i.e., $\delta$=0).

### A1. Solubility model

Initial conditions and tracer sources and sinks are simple in the solubility model. Initial conditions for DIC and $DI^{13}C$ in the ocean do not affect the final solution because the ocean equilibrates with an atmospheric reservoir of infinite size. There are no internal sources or sinks so that $\Gamma(C) = 0$. Dissolved organic carbon concentrations are zero. Total alkalinity is a linear function of salinity.

### A2. OBM

The conservation equation for $DI^{13}C$ differs from that for DIC because of $^{13}C$ fractionation from $^{12}C$ during photosynthesis and the production of dissolved and particulate organic $^{13}C$ ($DO^{13}C$ and $PO^{13}C$, respectively) and fractionation during the precipitation of $Ca^{13}CO_3$

$$\Gamma(DI^{13}C) = -J(PO^{13}C) - J(Ca^{13}CO_3) - \Gamma(DO^{13}C)\,. \qquad \text{(A4)}$$

The cycling of $^{13}C$ in POC is based on $J$(POP) and on the fractionation factor for photosynthesis from *Freeman and Hayes* [1992]. The equations for the cycling of $PO^{13}C$ parallel those for POP given by *Murnane et al.* [1999, Equation A6]:

$$J(PO^{13}C) = {}^{13}\Pi(1-\delta_z)(1-\sigma) - \delta_z\frac{\partial F_{PO^{13}C}}{\partial z} \qquad \text{(A5a)}$$

$${}^{13}\Pi = r_{C:P}\Pi\left[-0.0119\log\left(\left(CO_2\right)_{oc} + 0.9982\right)\right]\frac{\left({}^{13}CO_2\right)_{oc}}{\left(CO_2\right)_{oc}} \qquad \text{(A5b)}$$

$$F_{PO^{13}C} = {}^{13}F_{Z_e}\left(\frac{z}{z_e}\right)^{-0.858} \qquad \text{(A5c)}$$

$$^{13}F_{z_e}=(1-\sigma)\int_0^{z_e} {}^{13}\Pi dz \qquad \text{(A5d)}$$

where $\delta_z$ is set to 0 in the upper two "euphotic" layers of the model and has a value of 1 below that. The first term on the right-hand side of (A5a) is the production of organic $^{13}C$ in the photic zone of the model. Production of dissolved and particulate organic $^{13}C$ in the euphotic zone is given by $^{13}\Pi$. Equation (A5b) is based on the model predictions of phosphate new production, $\Pi$, which is defined by *Murnane et al.* [1999]. The fraction of new production put into labile dissolved organic matter is specified by sigma, which is set equal to 0.5. The fraction of the total production that goes into POP is specified by $(1-\sigma)$.

The second term on the right-hand side of (A5a) is remineralization of $PO^{13}C$ which occurs only below 119 m (the top of the third level) where $\delta_z$ is set to 1. $F_{PO^{13}C}$ is the flux of $PO^{13}C$ as a function of depth as specified by (A5c) obtained from sediment trap observations by *Martin et al.* [1987]. Remineralization of $PO^{13}C$ occurs immediately below where it is formed. The flux of $PO^{13}C$ at the base of the euphotic zone ($z_e$ = 119 m) specified by (A5d) is equal to the vertically integrated production of $PO^{13}C$ within the euphotic zone.

The conservation equation for $DO^{13}C$ parallels Equation (A7) for LDOC from *Murnane et al.* [1999]

$$\Gamma(DO^{13}C) = \sigma^{13}\Pi(1-\delta_z) - \kappa\delta_{do}[DO^{13}C]\,. \qquad \text{(A6)}$$

The first term on the right of (A6) is $LDO^{13}C$ production in the euphotic zone above 119 m, and the second term is $LDO^{13}C$ remineralization. The $\delta_{do}$ term is 1 when LDOC > 0 and 0 when LDOC ≤ 0. $LDO^{13}C$ is transported away from the region of production as a passive tracer following the water motion. Remineralization occurs as a first-order decay process at all depths unless LDOC ≤ 0. There is no fractionation of $^{13}C$ from $^{12}C$ during remineralization of LDOC or POC, and the same rate constant, $\kappa$, is used for LDOC and $LDO^{13}C$ remineralization.

The total alkalinity conservation equation for the OBM accounts for the cycling of nitrate and carbonate due to the biological model. The cycling of $^{13}C$ due to carbon cycling is derived from the TA conservation equation described by *Murnane et al.* [1999, Equations A8 and A9]. Carbonate precipitation fractionates $^{13}C$ from $^{12}C$ in the model, but there is no fractionation during dissolution. The change in $DI^{13}C$ due to carbonate cycling, $J(Ca^{13}CO_3)$, is based on the diagnosed $H^{13}CO^-_3$ and $HCO^-_3$, the predicted carbonate fluxes, and a fractionation factor for the formation of calcite (Table A1):

$$J(Ca^{13}CO_3) = {}^{13}\Phi + {}^{13}\Delta \qquad \text{(A7a)}$$

$$^{13}\Phi = \delta_a R_{C:P}(1-\delta_z)(1-\sigma)\Pi\frac{[H^{13}CO^-_3]}{[HCO^-_3]}\left(\frac{-4.185}{T(k)}+1.01493\right) \qquad \text{(A7b)}$$

$$^{13}\Delta = \delta_a R_{Ca:P}\delta_z\frac{\partial F_{POP}}{\partial z}\frac{\int_0^{z_e} {}^{13}\Phi dz}{\int_0^{z_e}\delta_a R_{Ca:P}(1-\delta_z)(1-\sigma)\Pi dz} \qquad \text{(A7c)}$$

The first term on the right side of Equation (A7a) gives the precipitation of $Ca^{13}CO_3$, the second gives the dissolution of $Ca^{13}CO_3$. The precipitation of $Ca^{13}CO_3$ is based on phosphate new production, $\Pi$, and $R_{Ca:P}$, the ratio of the global horizontal mean sources minus sinks of $CaCO_3$ to the global horizontal mean of sources minus sinks of particulate organic phosphorous. Dissolution of $Ca^{13}CO_3$ is based on $R_{Ca:P}$, the change in particulate organic phosphorous flux as a function of depth, $\partial F_{POP}/\partial z$, and the ratio of $Ca^{13}CO_3$ to $CaCO_3$ production in the photic zone of the model at a given latitude and longitude.

The $\delta_a$ parameter in (A7) is 1 unless any of several conditions are violated, in which case $0 \le \delta_a < 1$. The conditions that must be satisfied are (1) in levels 1 and 2 there must be formation of $CaCO_3$ and (2) in level three to twelve there can only be dissolution of $CaCO_3$. If either of these conditions is violated at any level, $\delta_a$ is set to 0 for that level. (3) A final condition is that the vertically integrated dissolution of $CaCO_3$ at any given latitude and longitude must be less than or equal to the production in the top levels. This condition is checked beginning with the third layer and adding one layer at a time moving downward. As long as the integrated dissolution is less than the production, $\delta_a$ is set to 1. If a level is reached where the integrated dissolution exceeds the production, then $\delta_a$ is set to a fraction between 0 and 1, such that the total dissolution equals exactly the production at the surface and all deeper levels have $\delta_a$ set to 0. Any excess $CaCO_3$ production is assumed to be lost to the sediments.

In addition to air-sea gas fluxes, there is a "virtual" flux at the surface of the ocean for each passive tracer that results from the way that precipitation and evaporation are handled in the model [*Murnane et al.*, 1999]. Freshwater fluxes are not modeled explicitly in the primitive equation ocean circulation model because the rigid lid approximation requires that ocean volume be conserved at each grid box. A full description of the virtual flux and its derivation are given by *Murnane et al.* [1999]. The constants used to calculate the virtual flux of $DI^{13}C$ and $LDO^{13}C$ are listed in Table A2 of *Murnane et al.* [1999].

**Acknowledgments.** The models described in this study were developed with support from Sea Grant via the New Jersey Marine Sciences Consortium (R/M-2), EPRI (RP8011-17 and RP8020-04), DOE (DE-FG02-90ER61052), NSF (OCE-9012333, OCE-9314707, and OCE-9726091), and NOAA (NA56GP0439). We gratefully acknowledge computer support from GFDL/NOAA through the generosity of J. Mahlman. We thank M. Bruno for the spline fits of atmospheric $\delta^{13}C$ data and C. LeQuéré for help with the anthropogenic transient model runs. S.-M. Fan graciously provided the atmospheric model results. The paper was improved with the help of comments by several anonymous reviewers.

## References

Aumont, O., Étude du cycle naturel du carbone dans un modè 3D de 1, océan mondial, Ph.D., Université Paris Vi, Paris, France, 1998.

Bacastow, R. B., and E. Maier-Reimer, Ocean-circulation model of the carbon cycle, *Clim. Dyn.*, *4*, 95-125, 1990.

Bacastow, R., and E. Maier-Reimer, Dissolved organic carbon in modeling oceanic new production, *Global Biogeochem. Cycles*, *5*, 71-85, 1991.

Bacastow, R. B., C. D. Keeling, T. J. Lucker, M. Wahlen, and W. G. Mook, The $^{13}C$ Suess effect in the world surface oceans and its implications for oceanic uptake of $CO_2$: Analysis of observations at Bermuda, *Global Biogeochem. Cycles*, *10*, 335-346, 1996.

Broecker, W. S., and E. Maier-Reimer, The influence of air and sea exchange on the carbon isotope distribution in the sea, *Global Biogeochem. Cycles*, *6*, 315-320, 1992.

Broecker, W. S., and T.-H. Peng, Interhemispheric transport of carbon dioxide by ocean circulation, *Nature*, *356*, 587-589, 1992.

Broecker, W. S., and T.-H. Peng, Evaluation of the $^{13}C$ constraint on the uptake of fossil fuel $CO_2$ by the ocean, *Global Biogeochem. Cycles*, *7*, 619-626, 1993.

Ciais, P., P. P. Tans, M. Trolier, J. W. C. White, and R. J. Francey, A large Northern Hemisphere terrestrial $CO_2$ sink indicated by the $^{13}C/^{12}C$ ratio of atmospheric $CO_2$, *Science*, *269*, 1098-1102, 1995.

Dickson, A. G., Thermodynamics of the dissociation of boric acid in synthetic seawater from 273.15 to 318.15 K, *Deep Sea Res.*, *37*, 755-766, 1990.

Dickson, A. G., and J. P. Riley, The estimation of acid dissociation constants in seawater media from potentiometric titrations with strong base, I, The ionic product of water - $K_W$, *Mar. Chem.*, *7*, 89-99, 1979a.

Dickson, A. G., and J. P. Riley, The estimation of acid dissociation constants in seawater media from potentiometric titrations with strong base, II, The dissociation of phosphoric acid, *Mar. Chem.*, *7*, 101-109, 1979b.

Esbensen, S. K., and Y. Kushnir, The heat budget of the global ocean: An atlas based on estimates from surface marine observations, *Clim. Res. Inst. Rep. 29*, Oregon State Univ., Corvallis, 1981.

Francey, R. J., P. P. Tans, C. E. Allison, I. G. Enting, J. W. C. White, and M. Trolier, Changes in oceanic and terrestrial carbon uptake since 1982, *Nature*, *373*, 326-330, 1995.

Francey, R. J., C. E. Allison, D. M. Etheridge, C. M. Trudinger, I. G. Enting, M. Leuenberger, R. L. Langenfelds, E. Michel, and L. P. Steele, A 1000 year high precision record of $\delta^{13}C$ in atmospheric $CO_2$, *Tellus, Ser. B.*, *51*, 170-193, 1999.

Freeman, K. H., and J. M. Hayes, Fractionation of carbon isotopes by phytoplankton and estimates of ancient $CO_2$ levels, *Global Biogeochem. Cycles*, *6*, 185-198, 1992.

Friedli, H., H. Lötscher, H. Oeschger, U. Siegenthaler, and B. Stauffer, Ice core record of the $^{13}C/^{12}C$ ratio of atmospheric carbon dioxide in the past two centuries, *Nature*, *324*, 237-238, 1986.

Goericke, R., and B. Fry, Variations of marine plankton $\delta^{13}C$ with latitude, temperature, and dissolved $CO_2$ in the world ocean, *Global Biogeochem. Cycles*, *8*, 85-90, 1994.

Goyet, C., and A. Poisson, New determination of carbonic acid dissociation constants in seawater as a function of temperature and salinity, *Deep Sea Res.*, *36*, 1635-1654, 1989.

Heimann, M., and E. Maier-Reimer, On the relations between the oceanic uptake of $CO_2$ and its carbon isotopes, *Global Biogeochem. Cycles*, *10*, 89-110, 1996.

Hellerman, S., and M. Rosenstein, Normal monthly wind stress over the world ocean with error estimates, *J. Phys. Oceanogr.*, *13*, 1093-1104, 1983.

Keeling, C. D., W. G. Mook, and P. Tans, Recent trends in the $^{13}C/^{12}C$ ratio of atmospheric carbon dioxide, *Nature*, *277*, 121-123, 1979.

Keeling, C. D., R. B. Bacastow, A. F. Carter, S. C. Piper, T. P. Whorf, M. Heimann, W. G. Mook, and H. Roeloffzen, A three-dimensional model of atmospheric $CO_2$ transport based on observed winds, 1, Analysis of observation data, in *Aspects of Climate Variability in the Pacific and the Western Americas, Geophys. Monogr. Ser.*, vol. 55, edited by D. H. Peterson, pp. 165-236, AGU, Washington D.C., 1989a.

Keeling, C. D., S. C. Piper, and M. Heimann, A three-dimensional model of atmospheric $CO_2$ transport based on observed winds, 4, Mean annual gradients and interannual variations, in *Aspects of Climate Variability in the Pacific and the Western Americas, Geophys. Monogr. Ser.*, vol. 55, edited by D. H. Peterson, pp. 305-363, AGU, Washington D.C., 1989b.

Keeling, C. D., and T. P. Whorf, Mauna Loa, in *Trends '91: A Compendium of Data on Global Change*, edited by T. A. Boden, R. J. Sepanski, and F. W. Stoss, pp. 12-14, Carbon Dioxide Inf. Anal. Cent., Oak Ridge Nat. Lab., Oak Ridge, Tenn., 1991.

Keeling, C. D., T. P. Whorf, M. Wahlen, and J. van der Plicht, Interannual extremes in the rate of rise of atmospheric carbon dioxide since 1980, *Nature*, *375*, 666-670, 1995.

Keeling, R. F., and T.-H. Peng, Transport of heat, $CO_2$ and $O_2$ by the Atlantic's thermohaline circulation, *Philos. Trans. R. Soc. London, Ser. B*, *348*, 133-142, 1995.

Khoo, K. H., R. W. Ramette, C. H. Culberson, and R. G. Bates, Determination of hydrogen ion concentrations in seawater from 5 to 40°C: Standard potentials at salinities from 20 to 45‰, *Anal. Chem.*, *49*, 29-34, 1977.

Leuenberger, M., Isotopen-sowie Konzentrationsbestimmungen an $CO_2$, $N_2O$, $O_2$ und $N_2$ in Luftproben aus polarem Eis, Ph.D. thesis, Univ. of Bern, Bern, Switzerland, 1992.

Levitus, S., *Climatological Atlas of the World Ocean, NOAA Prof. Pap.*, *13*, 173 pp., U. S. Dep. of Commer., Rockville, Md., 1982.

Lynch-Stieglitz, J., T. F. Stocker, W. S. Broecker, and R. G. Fairbanks, The influence of air-sea exchange on the isotopic composition of oceanic carbon: Observations and modeling, *Global Biogeochem. Cycles*, *9*, 653-665, 1995.

Mackensen, A., H.-W. Hubberten, T. Bickert, G. Fischer, and D. K. Fütterer, The $\delta^{13}C$ in benthic foraminiferal test of *Fontmotia Wuellerstorfi* (Schwager) relative to the $\delta^{13}C$ of dissolved inorganic carbon in Southern Ocean deep water: Implications for glacial ocean circulation models, *Paleoceanography*, *8*, 587-610, 1993.

Mahlman, J. D., and W. J. Moxim, Tracer simulation using a global general circulation model: Results from a mid-latitude instantaneous source experiment, *J. Atmos. Sci.*, *35*, 1340-1374, 1978.

Maier-Reimer, E., and K. Hasslemann, Transport and storage of $CO_2$ in the ocean - An inorganic ocean-circulation carbon cycle model, *Clim. Dyn.*, *2*, 63-90, 1987.

Martin, J. H., G. A. Knauer, D. M. Karl, and W. W. Broenkow, VERTEX: Carbon cycling in the northeast Pacific, *Deep Sea Res.*, *34*, 267-285, 1987.

Mook, W. G., $^{13}C$ in atmospheric $CO_2$, *Neth. J. of Sea Res.*, *20*, 211-223, 1986.

Murnane, R. J., J. L. Sarmiento, and C. L. Quéré, Spatial distribution of air-sea $CO_2$ fluxes and the interhemispheric transport of carbon by the oceans, *Global Biogeochem. Cycles*, in press, 1999.

Neftel, A., E. Moor, H. Oeschger, and B. Stauffer, Evidence from polar ice cores for the increase in atmospheric $CO_2$ in the past two centuries, *Nature*, *315*, 45-47, 1985.

Ostlund, H. G., H. Craig, W. S. Broecker, and D. Spencer, *GEOSECS Atlantic, Pacific, and Indian Ocean Expeditions, Vol. 7, Shorebased Data and Graphics*, Nat. Sci. Found., Washington, D.C., 1987.

Pacanowski, R., K. Dixon, and A. Rosati, The G.F.D.L. Modular Ocean Model Users Guide, *GFDL Ocean Group Tech. Rep. 2*, Geophys. Fluid Dyn. Lab., 1993.

Peng, T. H., T. Takahashi, and W. S. Broecker, Seasonal variability of carbon dioxide, nutrients and oxygen in the northern Atlantic surface water: Observations and a model, *Tellus, Ser. B*, *39*, 439-458, 1987.

Quay, P. D., B. Tilbrook, and C. S. Wong, Oceanic uptake of fossil fuel $CO_2$: Carbon-13 evidence, *Science*, *256*, 74-79, 1992.

Quinby-Hunt, M. S., and K. K. Turekian, Distribution of elements in sea water, *EOS Trans. AGU*, *64*, 130-131, 1983.

Rau, G. H., U. Riebesell, and D. Wolf-Gladrow, $CO_{2aq}$-dependent photosynthetic $^{13}C$ fractionation in the ocean: A model versus measurements, *Global Biogeochem. Cycles*, *11*, 267-278, 1997.

Rubinson, M., and R. N. Clayton, Carbon-13 fractionation between aragonite and calcite, *Geochim. Cosmochim. Acta*, *33*, 997-1002, 1969.

Sarmiento, J. L., R. Monfray, E. Maier-Reimer, O. Aumont, R. J. Murnane, and J. Orr, Sea-air $CO_2$ fluxes and carbon transport: A comparison of three ocean general circulation models, *Global Biogeochem. Cycles*, in press, 1999.

Sarmiento, J. L., J. C. Orr, and U. Siegenthaler, A perturbation simulation of $CO_2$ uptake in an ocean general circulation model, *J. Geophys. Res.*, *97*, 3621-3646, 1992.

Sarmiento, J. L., R. Murnane, and C. L. Quéré, Air-sea $CO_2$ transfer and the carbon budget of the North Atlantic, *Philos. Trans. R. Soc. London, Ser. B, 348*, 211-219, 1995.

Schimel, D., I. G. Enting, M. Heimann, T. M. L. Wigley, D. Raynaud, D. Alves, and U. Siegenthaler, $CO_2$ and the Carbon Cycle, in *Climate Change 1994*, edited by J. T. Houghton et al., pp. 35-71, Cambridge Univ. Press, New York, 1995.

Siegenthaler, U., and F. Joos, Use of simple model for studying oceanic tracer distributions and the global carbon cycle, *Tellus, Ser. B, 44B*, 186-207, 1992.

Siegenthaler, U., and K. O. Münnich, $^{13}C/^{12}C$ fractionation during $CO_2$ transfer from air to sea, in *Carbon Cycle Modelling*, edited by B. Bolin, pp. 249-257, John Wiley, New York, 1981.

Sjoberg, S., A. Nordin, and N. Ingri, Equilibrium and structu16 studies of silicon(IV) and aluminium(III) in aqueous solution II> Formation constants for the monosilicate ions $SiO(OH)^-_3$ and $SiO_2(OH)^{2-}_2$: A preci-

sion study at 25°C in a simplified seawater medium, *Mar. Chem.*, *10*, 521-532, 1981.

Stephens, B. B., R. F. Keeling, M. Heimann, K. K. Six, R. Murnane, and K. Caldiera, Testing global ocean carbon cycle models using measurements of atmospheric $O_2$ and $CO_2$ concentrations, *Global Biogeochem. Cycles*, *12*, 213-230, 1998.

Tans, P. P., J. A. Berry, and R. F. Keeling, Oceanic $^{13}C/^{12}C$ observations: A new window on ocean $CO_2$ uptake, *Global Biogeochem. Cycles*, *7*, 353-368, 1993.

Toggweiler, J. R., K. Dixon, and K. Bryan, Simulation of radiocarbon in a coarse-resolution world ocean model, 1, Steady state prebomb distributions, *J. Geophys. Res.*, *94*, 8217-8242, 1989a.

Toggweiler, J. R., K. Dixon, and K. Bryan, Simulations of radiocarbon in a coarse-resolution world ocean model, 2, Distributions of bomb-produced carbon 14, *J. Geophys. Res.*, *94*, 8243-8264, 1989b.

Toggweiler, J. R., and B. Samuels, Is the magnitude of the deep outflow from the Atlantic Ocean actually governed by southern hemisphere winds?, in *The Global Carbon Cycle*, edited by M. Heimann, pp. 303-331, Springer-Verlag, New York, 1993a.

Toggweiler, J. R., and B. Samuels, New radiocarbon constraints on the upwelling abyssal water to the ocean's surface, in *The Global Carbon Cycle*, edited by M. Heimann, pp. 333-366, Springer-Verlag, New York, 1993b.

Trolier, M., J. W. C. White, P. P. Tans, K. A. Masarie, and P. A. Gemery, Monitoring the isotopic composition of atmospheric $CO_2$: Measurements from the NOAA Global Air Sampling Network, *J. Geophys. Res.*, *101*, 25,897-25,916, 1996.

Uppström, L. R., The boron/chlorinity ratio of deep-sea water from the Pacific Ocean, *Deep Sea Res.*, *21*, 161-162, 1974.

Volk, T., and M. I. Hoffert, Ocean carbon pumps: Analysis of relative strengths and efficiencies in ocean-driven atmospheric $CO_2$ changes, in *The Carbon Cycle and Atmospheric $CO_2$: Natural Variations Archean to Present, Geophys. Monogr. Ser.* vol. 32, edited by E. T. Sundquist and W. S. Broecker, pp. 99-110, AGU, Washington, D. C., 1985.

Volk, T., and Z. Liu, Controls of $CO_2$ sources and sinks in the Earth scale surface ocean: Temperature and nutrients, *Global Biogeochem. Cycles*, *2*, 73-89, 1988.

Wanninkhof, R., Relationship between wind speed and gas exchange over the ocean, *J. Geophys. Res.*, *97*, 7373-7383, 1992.

R. J. Murnane, Risk Prediction Initiative, Bermuda Biological Station for Research, Ferry Reach, St. George's, GE01, Bermuda. (rmurnane@bbsr.edu)

J. L. Sarmiento, Program in Atmospheric and Oceanic Sciences, Department of Geosciences, Princeton University, Princeton, NJ 08544.

(Received July 29, 1998; revised October 4, 1999;
accepted October 11, 1999.)